

## A frequency tracking semi-active algorithm for control of edgewise vibrations in wind turbine blades

John Arrigan<sup>1</sup>, Chaojun Huang<sup>2</sup>, Andrea Staino<sup>1</sup>, Biswajit Basu<sup>\*1</sup> and Satish Nagarajaiah<sup>2</sup>

<sup>1</sup>Department of Civil, Structural and Environmental Engineering, Trinity College Dublin, Ireland

<sup>2</sup>Department of Civil and Env. Eng. and Mech. Eng. and Mat. Sc., Rice University, Houston, TX, USA

(Received February 10, 2012, Revised August 18, 2012, Accepted February 4, 2013)

**Abstract.** With the increased size and flexibility of the tower and blades, structural vibrations are becoming a limiting factor towards the design of even larger and more powerful wind turbines. Research into the use of vibration mitigation devices in the turbine tower has been carried out but the use of dampers in the blades has yet to be investigated in detail. Mitigating vibrations will increase the design life and hence economic viability of the turbine blades and allow for continual operation with decreased downtime. The aim of this paper is to investigate the effectiveness of Semi-Active Tuned Mass Dampers (STMDs) in reducing the edgewise vibrations in the turbine blades. A frequency tracking algorithm based on the Short Time Fourier Transform (STFT) technique is used to tune the damper. A theoretical model has been developed to capture the dynamic behaviour of the blades including the coupling with the tower to accurately model the dynamics of the entire turbine structure. The resulting model consists of time dependent equations of motion and negative damping terms due to the coupling present in the system. The performances of the STMDs based vibration controller have been tested under different loading and operating conditions. Numerical analysis has shown that variation in certain parameters of the system, along with the time varying nature of the system matrices has led to the need for STMDs to allow for real-time tuning to the resonant frequencies of the system.

**Keywords:** structural control; vibration; semi-active control; damping; wind energy

---

### 1. Introduction

Since the early 1990s huge growth has been seen in the wind energy sector. Single turbines with outputs as large as 5MW are now being constructed with tower heights and blade diameters of over 80 m and 120 m respectively. With the continual increasing size of wind turbines, the blades are becoming more and more flexible making it important to understand and control their dynamic behaviour. A considerable amount of research has been carried out into wind turbine blade design (Bechly and Clausen (1997), Jensen *et al.* (2006), Shokrieh and Rafiee (2006), Staino *et al.* (2012)). However, it is only recently with the increased size and flexibility of wind turbine blades that their dynamic behaviour has become a major research area. Ahlström (2006) carried

---

\*Corresponding author, Professor, E-mail: basub@tcd.ie

out one such study investigating the effect of increased flexibility in wind turbine blades and found that it can lead to a significant fall in power output.

There are two main types of vibration that occur in wind turbine blades; flapwise and edgewise. Flapwise vibrations are vibrations that occur out of the plane of rotation of the blades and edgewise vibrations are vibrations occurring in the plane of rotation. Nearly all the research thus far carried out into wind turbine blade dynamics has focused on flapwise vibration. Ronold and Larsen (2000) studied the failure of a wind turbine blade in flapwise bending during normal operating conditions of the turbine. Ronold *et al.* (1999) developed a probabilistic model for analysis of the safety of wind turbine blades against failure in the flapwise direction. Murtagh *et al.* (2005) derived a model of a wind turbine including blade (flapwise motion)-tower interaction. On comparing their model to a model which omitted the dynamic coupling, they found that inclusion of blade tower interaction resulted in increases in the maximum blade tip displacement of up to 256% depending on the rotational speed of the turbine. Staino and Basu (2011) investigated the effect of uncertainty on the flapwise vibration of rotor blades and proposed robust control strategies.

In the last few years since the problem of severe edgewise vibrations became apparent in some turbines, research has been carried out investigating their occurrence. Thomsen *et al.* (2000) noted that edgewise vibrations were stall-induced and due to the fact that the total damping of the blades in the edgewise direction becomes negative. This is a result of several factors, including the structural dynamics of the wind turbine and the blade airfoil characteristics. They stated that the problem of edgewise vibration was difficult to predict and thus proposed a method for determining the structural damping present in a blade under edgewise vibration. They achieved this by exciting a full scale blade in its edgewise modes and determined the damping from the decay of the mode amplitudes. Chaviaropoulos (2001) noted the occurrence of violent edgewise vibrations in turbine blades and developed a numerical tool for investigating the aeroelastic stability of a wind turbine blade under combined flapwise/edgewise motion. Hansen (2003) performed an extensive study into the dynamic behaviour of wind turbines and focused on edgewise vibrations. It was shown that edgewise vibrations are less damped than their flapwise counterparts and concluded that blade vibrations are strongly affected by the dynamics of the shaft, nacelle and tower. Some research has been carried out in an attempt to counteract the increased vibration problems seen in wind turbine blades. This has focused on the actual design of the blades themselves by trying to increase the structural damping inherently present in them or alter their aerodynamic characteristics (Chaviaropoulos *et al.* (2003), Chaviaropoulos *et al.* (2006)). Thus far little research has been performed into investigating the possibility of using dampers in the blades.

Tuned mass dampers (TMDs) are vibration mitigating devices consisting of a mass connected by a spring and a dashpot to the primary structure. By tuning the frequency of the TMDs to the resonant frequencies of the structural system being damped, vibrations in the main structure can be significantly reduced through the out-of-phase motion of the damper relative to the primary system. The use of passive TMDs for wind turbine applications has been investigated in Murtagh *et al.* (2008) and Lackner and Rotea (2011). Over the last few decades extensive research has been carried out into the use of passive TMDs and their suitability for vibration control (Chang (1999), Hijmissen and van Horssen (2007), Kareem and Kline (1995), Li and Ni (2007)). However, due to the non-linearity of nearly all engineering dynamical systems, research has more recently focused on Semi-Active TMDs (STMDs) due to their adaptive capabilities without the need for directly injecting energy into the primary structure, even though a very small amount of energy is still required (semi-active devices need external power to change the properties of the spring and/or

damper). Arrigan *et al.* (2011) considered the use of STMDs for reducing vibrations in the flapwise direction in wind turbines. Pinkaew and Fujino (2001) studied the use of STMDs for vibration suppression in harmonically excited structures and compared their performance to a standard TMD. Nagarajaiah (2009) and Nagarajaiah and Varadarajan (2005) have developed algorithms to track the dominant frequency of the system using a Short Time Fourier Transform (STFT) technique. This enabled their STMD to be continuously tuned to the dominant frequency of the structure resulting in a significantly improved response than that achieved by a conventional passive TMD. Nagarajaiah and Sonmez (2007) developed algorithms using an STFT technique for control of multiple STMDs in multi-storey structures.

The aim of this paper is to investigate the use of STMDs in the vibration control of wind turbine blades. Wind turbine blades are automatically suitable for the installation of vibration mitigating devices due to their hollow nature. However, thus far little or no work has been done on investigating the potential use of dampers for vibration control in these fatigue critical components. The theoretical model developed in this paper considers only the structural dynamics of the blades including their interaction with the nacelle/tower of the turbine. Negative damping occurs in the model due to the dynamic interaction between the blades and nacelle in accordance with Thomsen *et al.* (2000) study. The model developed consists of three rotating cantilever beams with variable mass and stiffness per unit length (representing the turbine blades) connected at their root to a large mass (which represents the nacelle) free to move in the horizontal edgewise direction. Realistic structural and aerodynamic data from the NREL 5-MW baseline wind turbine were considered for the tuning of the dynamic simulation model. The damping configuration studied looked at installing a STMD in each blade tip and at the nacelle giving the final model 8 Degrees of Freedom (DOF). Different operating conditions of the turbine, loading scenarios and parametric variations have been simulated to investigate the flexibility and the robustness of the proposed control algorithm. Turbulent wind loading acting along the turbine blades was considered in the analysis. The study focused on the edgewise vibrations only.

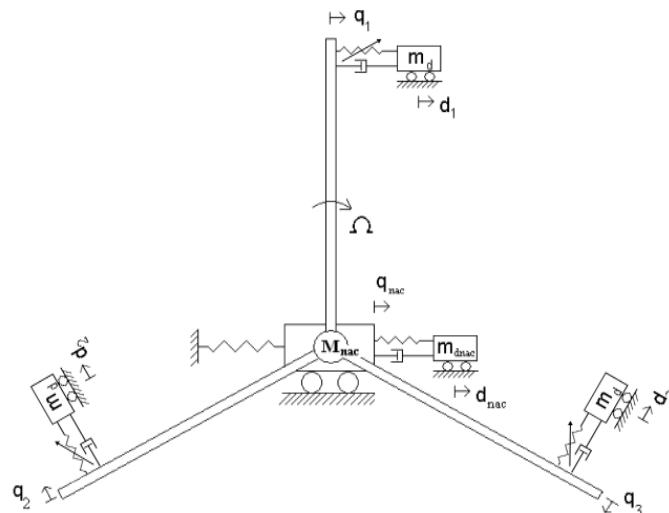


Fig. 1 Dynamic model of the system with STMDs

## 2. Analysis

### 2.1 Model formulation

A dynamic model of the turbine was formulated to capture the structural interaction between the blades and the nacelle. Each blade was modeled as a rotating cantilever beam with variable mass and stiffness along the length. These were attached at their root to a large mass equal to that of the nacelle, which was free to move in the horizontal direction. Structural damping has been added to the model in the form of stiffness proportional damping. Four variable stiffness STMDs were attached to the model, one at each blade tip and one at the nacelle. The dampers were modeled as simple mass-spring-dashpot systems. The stiffness of the spring could be altered according to the semi-active algorithm developed later in this paper. A schematic of the model is shown in Fig. 1.

The final model with all STMDs included consists of 8 DOF where  $q_1$ ,  $q_2$  and  $q_3$  represent the blade tip displacements, with  $d_1$ ,  $d_2$  and  $d_3$  representing the STMDs attached to each of the blades. The motion of the nacelle and nacelle STMD were represented by  $q_{nac}$  and  $d_{nac}$  respectively. An appropriate function approximation was computed from the eigen-analysis of the blade structural data in order to represent the fundamental mode shape  $\Phi(x)$  of the beam. The rotational speed of the blades is labelled in Fig. 1 as  $\Omega$ . The undamped equations of motion for the system were first formulated using the Lagrangian formulation outlined in Eq. (1).

$$\frac{d}{dt} \left( \frac{\partial T}{\partial \dot{q}_i} \right) - \frac{\partial T}{\partial q_i} + \frac{\partial V}{\partial q_i} = Q_i \quad , \quad i = 1 \dots 4 \quad (1)$$

where:  $T$  = kinetic energy of the system,  $V$  = potential energy of the system,  $q_i$  = displacement of degree of freedom  $i$  and  $Q_i$  = generalized loading for degree of freedom  $i$ . The kinetic and potential energies of the model  $T$  and  $V$  respectively were first derived and are stated in Eqs. (2(a) and 2(b)). These expressions were then substituted back into the Lagrangian formulation in Eq. (1) to allow the equations of motion to be determined.

$$T = \frac{1}{2} \sum_{i=1}^3 \int_0^L \mu(x) v_{bi}^2 dx + \frac{1}{2} M_{nac} \dot{q}_{nac}^2 \quad (2a)$$

$$V = \frac{1}{2} \sum_{i=1}^3 \int_0^L \left[ EI(x) \left( \frac{\partial^2 u_i}{\partial x^2} \right)^2 + F_c(x) \left( \frac{\partial u_i}{\partial x} \right)^2 \right] dx + \frac{1}{2} K_{nac} q_{nac}^2 \quad (2b)$$

where:  $\mu(x)$  = mass per unit length,  $L$  = length of the blade,  $v_{bi}$  = velocity of blade ' $i$ ' including rotation and the nacelle motion that causes blade displacement,  $M_{nac}$  = mass of nacelle,  $\dot{q}_{nac}$  = velocity of nacelle,  $E$  = Young's Modulus for the blade,  $I(x)$  = second moment of area of blade,  $K$  = stiffness of the nacelle,  $u_i$  is the displacement of the blade  $i$  and  $q_{nac}$  is the displacement of the nacelle as shown above in Fig. 1. In Eq. (2(b)), to accurately model the structural dynamic behaviour of a wind turbine, centrifugal stiffening of the blades was also included, as the stiffness of the blades increases at higher rotational speeds. Considering elements of size  $d\xi$  along the blade and integrating over the length, the centrifugal force on blade acting at the point ' $x$ ' from the hub is

$$F_c(x) = \Omega^2 \int_x^L \mu(\xi) \xi d\xi \quad (3)$$

where ‘ $\xi$ ’ is the distance from ‘ $x$ ’ to the current element considered.

The subsequent equations of motion for the 4 DOF undamped model are stated below in Eq. (4) before the addition of the stiffness proportional structural damping. The equations of motion for the model with the STMDs was then determined using the same technique as before by deriving the expressions for the kinetic and potential energies (this time with the dampers attached), and re-applying the Lagrangian formulation as stated in Eq. (1).

$$\begin{bmatrix} m_2 & 0 & 0 & m_1 \cos(\Omega t) \\ 0 & m_2 & 0 & m_1 \cos(\Omega t + \frac{2\pi}{3}) \\ 0 & 0 & m_2 & m_1 \cos(\Omega t + \frac{4\pi}{3}) \\ m_1 \cos(\Omega t) & m_1 \cos(\Omega t + \frac{2\pi}{3}) & m_1 \cos(\Omega t + \frac{4\pi}{3}) & M_{nac} + 3m_0 \end{bmatrix} \begin{bmatrix} \ddot{q}_1 \\ \ddot{q}_2 \\ \ddot{q}_3 \\ \ddot{q}_{nac} \end{bmatrix} + \begin{bmatrix} 0 & 0 & 0 & 0 \\ 0 & 0 & 0 & 0 \\ 0 & 0 & 0 & 0 \\ -2\Omega m_1 \sin(\Omega t) & -2\Omega m_1 \sin(\Omega t + \frac{2\pi}{3}) & -2\Omega m_1 \sin(\Omega t + \frac{4\pi}{3}) & 0 \end{bmatrix} \begin{bmatrix} \dot{q}_1 \\ \dot{q}_2 \\ \dot{q}_3 \\ \dot{q}_{nac} \end{bmatrix} + \begin{bmatrix} K_2 & 0 & 0 & 0 \\ 0 & K_2 & 0 & 0 \\ 0 & 0 & K_2 & 0 \\ -\Omega^2 m_1 \cos(\Omega t) & -\Omega^2 m_1 \cos(\Omega t + \frac{2\pi}{3}) & -\Omega^2 m_1 \cos(\Omega t + \frac{4\pi}{3}) & K_{nac} \end{bmatrix} \begin{bmatrix} q_1 \\ q_2 \\ q_3 \\ q_{nac} \end{bmatrix} = \begin{bmatrix} Q_1 \\ Q_2 \\ Q_3 \\ Q_{nac} \end{bmatrix} \quad (4)$$

where  $m_0$  = total (integrated) blade mass,  $m_1 = \int_0^L \mu(x) \Phi(x) dx$ ,  $m_2$  = modal mass of the blade.

In the stiffness matrix, the term  $K_2$  is defined as

$$K_2 = K_e + K_g - \Omega^2 m_2 \quad (5)$$

where  $K_e$  = generalized elastic stiffness of the blade and  $K_g$  = geometrical stiffness associated with the axial force (centrifugal stiffening).

It is important to note the time varying harmonic terms in the system matrices which are a result of the coupling between the nacelle and rotating blades. The damping matrix is of particular interest as although structural damping has yet to be included, negative time varying damping terms still arise. This is in accordance with Thomsen et al.’s study (Thomsen *et al.* 2000) mentioned earlier in the paper. If nacelle motion is not considered, these negative time varying damping terms do not occur indicating that they are purely a result of the dynamic interaction

between the blades and nacelle.

The addition of structural damping in the model is a complicated issue as in time varying systems it is something that is not well understood. Indeed in normal time invariant systems structural damping is something that can only be estimated. For the stationary turbine ( $\Omega=0$ ), time varying terms are eliminated so the presence of some structural damping can be assumed as in the case of a time invariant system. Therefore the structural damping assumed in the model is taken as stiffness proportional damping for the stationary turbine, i.e. proportional to the stiffness matrix for  $\Omega=0$ .

The effect of gravity was also included, as it has been found to have an influence on the edgewise vibration (Staino *et al.* (2012)). In this case, the stiffness term  $K_2$  in Eq. (5) for the  $i$ -th blade was computed as

$$K_2 = K_e + K_g - \Omega^2 m_2 + K_w \cos(\Omega t + \varphi_i) \quad (6)$$

where  $\varphi_i = \Omega t + (i-1) \frac{2\pi}{3}$ ,  $i=1,2,3$  and  $K_w$  denotes the stiffness arising out of gravity effects. The generalized load in Eq. (4) was also changed in order to include gravity loadings. The right-hand side of the turbine's equations of motion becomes

$$\begin{bmatrix} \bar{Q}_1 \\ \bar{Q}_2 \\ \bar{Q}_3 \\ \bar{Q}_{nac} \end{bmatrix} = \begin{bmatrix} Q_1 \\ Q_2 \\ Q_3 \\ Q_{nac} \end{bmatrix} + \begin{bmatrix} Q_{w,1} \\ Q_{w,2} \\ Q_{w,3} \\ 0 \end{bmatrix} \quad (7)$$

where the term  $Q_{w,i}$ ,  $i=1,2,3$  for the  $i$ -th blade represents the generalized load arising from gravitational effects and it is modeled as

$$Q_{w,i} = g \int_0^L \mu(x) \Phi(x) dx \sin(\Omega t + \varphi_i) \quad (8)$$

## 2.2 Aerodynamic loading

A realistic estimate of the wind loading was computed by applying the corrected Blade Element Momentum (BEM) method as found in Hansen (2008). The method takes into account the aerodynamic properties of the blade section airfoils, the geometrical characteristics of the rotor, the wind passing through the rotor swept area the rotational velocity of the blades. In the BEM framework, the blade is assumed to be discretized into a number of sections (elements), each located at a radial distance  $r$  from the hub. No aerodynamic interaction between different elements is assumed. The lift and drag forces acting on each blade segment are computed as

$$\begin{aligned} P_L(r,t) &= \frac{1}{2} \rho V_{rel}^2(r,t) c_r C_l(\alpha) \\ P_D(r,t) &= \frac{1}{2} \rho V_{rel}^2(r,t) c_r C_d(\alpha) \end{aligned} \quad (9)$$

where  $\rho$  = density of air,  $c_r$  = local chord length,  $V_{rel}$  = local relative wind velocity and  $C_l(\alpha)$ ,  $C_d(\alpha)$  represent the lift and drag coefficients, respectively, whose values depend on the local angle of attack. The aerodynamic load in the edgewise direction  $p_T(r,t)$  can be obtained by projecting the lift and the drag forces along the plane tangential to the rotor, according to the formula:

$$p_T(r,t) = p_L(r,t) \sin(\phi) - p_D(r,t) \cos(\phi) \quad (10)$$

where  $\phi$  = local flow angle, which determines the local angle of attack.

The local relative wind velocity in Eq. (9) is computed by considering the steady and the turbulent components of the wind velocity. In this paper, a steady wind load that varied with height was assumed to act on the blades. The rotation of the blades meant that the magnitude of this load acting on the blades varied with time, with a period corresponding to the rotor angular velocity  $\Omega$ . An isotropic, homogenous turbulence was then added to this steady wind component to represent a real life loading scenario. A 1-D fully coherent turbulence was generated at a height equal to that of the nacelle using a Kaimal spectrum (Kaimal *et al.* (1972)) defined by Eqs. (11), (12) and (13) below.

$$\frac{\omega S_{vv}(H, \omega)}{\sigma_v^2} = \frac{100c}{3(1+50c)^{\frac{5}{3}}} \quad (11)$$

where:  $H$  = nacelle height,  $S_{vv}(H, \omega)$  is the PSDF (Power Spectral Density Function) of the fluctuating wind velocity as a function of the hub elevation and frequency,  $\bar{v}(H)$  is the mean wind speed at the hub height as defined in Eq. (12),  $\sigma_v$  is the standard deviation of the wind speed and  $c$  is known as the Monin coordinate as in Eq. (13).

$$\bar{v}(H) = \frac{1}{k} v_* \log \frac{H}{z_0} \quad (12)$$

$$c = \frac{\omega H}{2\pi \bar{v}(H)} \quad (13)$$

In Eq. (12),  $k$  is Von-Karman's constant (typically around 0.4, Simiu and Scanlan (1996)),  $v_*$  is the friction velocity and  $z_0 = 0.005$  the roughness length. The generalized load on the nacelle resulted due to the dynamic coupling with the blades.

### 2.3 STFT based frequency tracking algorithm

STFT is a widely used technique to identify the time-frequency distribution of non-stationary signals. It allows the identification of local frequencies that exist only for a short period of time in the systems response. The signal is essentially split up into small time segments and each one is analyzed by a Fast Fourier Transform (FFT) to ascertain the current frequencies present in the signal. By combining each of these frequency spectra the time frequency distribution of the system can be attained.

#### 2.3.1 Short-time Fourier transform and spectrogram

The short-time Fourier transform is a mathematical tool devised for analyzing a signal in both

time and frequency. It is based on Fourier transform of a short (time-windowed) portion of signal  $s_h(\tau)$  sampled by a moving window  $h(\tau-t)$ . The running time is  $\tau$  and the fixed time is  $t$ . Since the time interval/window considered is short as compared to the signal this integral operator is termed as the STFT.

$$S_t(\omega) = \frac{1}{\sqrt{2\pi}} \int_{-\infty}^{\infty} s_h(\tau) e^{-j\omega\tau} d\tau \quad (14)$$

where  $s_h(\tau)$  is defined as follows

$$s_h(\tau) = s(\tau)h(\tau-t) \quad (15)$$

In Eq. (15),  $h(\tau-t)$  is an appropriately chosen window function that emphasizes or captures information about the signal around the time  $t$ , and is a function of  $t-\tau$ , i.e.,  $s_h(\tau) = s(\tau)$  for  $\tau$  near  $t$  and decays to  $s_h(\tau) = 0$  for  $\tau$  far away from  $t$ . Considering this signal as a function of  $\tau$  a spectrum of this function can be constructed. This spectrum will emphasize the presence of frequencies locally at time  $t$ . In particular the spectrum is

$$S_t(\omega) = \frac{1}{\sqrt{2\pi}} \int_{-\infty}^{\infty} s(\tau)h(\tau-t)e^{-j\omega\tau} d\tau \quad (16)$$

which is the STFT. The energy density of the modified signal and the time-frequency spectrogram is given by

$$P(t, \omega) = |S_t(\omega)|^2 \quad (17)$$

or

$$P_{SP}(t, \omega) = \left| \frac{1}{\sqrt{2\pi}} \int_{-\infty}^{\infty} s(\tau)h(\tau-t)e^{-j\omega\tau} d\tau \right|^2 \quad (18)$$

The limitation of STFT is its fixed resolution. In STFT the length of the signal segment chosen or the length of the windowing function  $h(t)$  determines the resolution: broad window results in better frequency resolution but poor time resolution, and narrow window results in good time resolution but poor frequency resolution, due to the time-bandwidth relation (uncertainty principle (Cohen 1995). More discussions on STFT are available in Nagarajaiah and Basu (2009).

### 2.3.2 STFT implementation procedure

The implementation procedure for the STFT in the discrete domain is carried out by extracting time windows of the original non-stationary signal  $s(t)$ . After zero padding and convolving the signal with Hamming window, the Discrete Fourier Transform (DFT) is computed for each windowed signal to obtain STFT,  $S_t(\omega)$ , of signal  $s_h(\tau)$ . If the window width is  $n\Delta t$  (where  $n$  is number of points in the window, and  $\Delta t$  is the sampling rate of the signal), the  $k$ -th element in  $S_t(\omega)$  is the Fourier coefficient that corresponds to the frequency

$$\omega_k = \frac{2\pi k}{n\Delta t}, \quad \text{for window width } n\Delta t \quad (19)$$

The STFT algorithm developed in this study allows the STMDs to be tuned in real-time to the

dominant frequencies in the system. Before each time segment is Fourier analyzed it is multiplied by a window function placed on the time window of interest. In this case the time window of interest is the windowed segment left of the current time of the response to allow for real-time tuning. A Hanning window is used to center on the current time, thus emphasizing the most recent frequencies present in the response of the turbine. Once the weighted signal is obtained an FFT is performed and the frequency spectrum obtained. The dominant frequencies in the current time segment are then identified and the STMDs tuned to these frequencies. The process is repeated every second allowing the tuning of the STMDs to be adjusted in real-time as the frequencies of the system change. The semi-active algorithm is illustrated in the flow chart in Fig. 2.

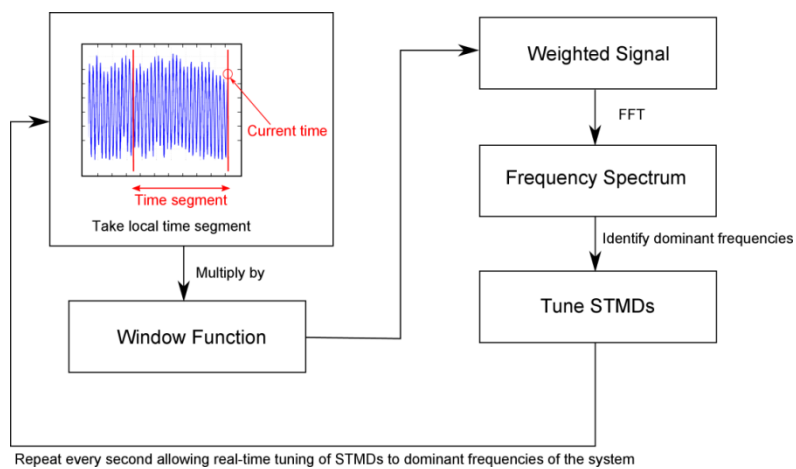


Fig. 2 Frequency tracking STFT based semi-active algorithm

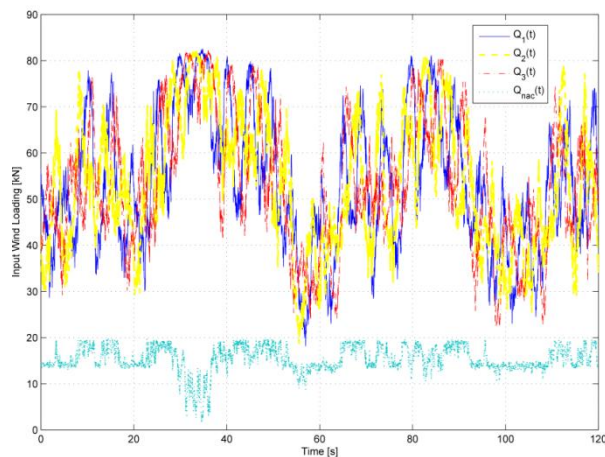


Fig. 3 Edgewise aerodynamic loads with 10% turbulence intensity

### 3. Numerical results

The proposed wind turbine model was tuned to simulate the dynamic response of a 5-MW wind turbine. Structural and aerodynamic data from the NREL offshore 5-MW baseline wind turbine as in Jonkman *et al.* (2009) were considered. The system parameters used in the numerical investigation are reported in Table 1.

Time history simulations were carried out on the model for the turbulent wind loading described previously. The time history of the edgewise input wind loads acting on blades and nacelle subjected to a steady wind with homogenous isotropic turbulence (10% intensity) is shown in Fig. 3. The response of the system was transformed to the frequency domain by an FFT to allow the main frequencies in the system to be determined. Fig. 4(a) shows the frequency plot for blade 1, while Fig. 4(b) shows the frequency response of the nacelle.

Table 1 Properties of NREL 5-MW Baseline HAWT

<b>Properties of the wind turbine with SMTDs</b>			
<b>Basic Description</b>	Max. Rated Power	5000 kW	
	Rotor Orientation, Configuration	Upwind, 3 Blades	
	Rotor Diameter	126 m	
	Hub Height	90 m	
	Rated Rotor Speed	12.1 rpm	
<b>Blade (LM 61.5 P2)</b>	Length	61.5 m	
	Overall (Integrated) Mass	17740 kg	
	Second Mass Moment of Inertia	11776 kgm <sup>2</sup>	
	1-st Edgewise Mode Natural Frequency	1.08 Hz	
	Structural-Damping Ratio	0.48%	
	TMD Mass Ratio	1%	
	TMD Damping Ratio	6.09%	
	TMD Fractional Distance from Blade Root	0.9	
	<b>Hub+Nacelle</b>	Hub Diameter	3 m
		Hub Mass	56780 kg
Nacelle Mass		240000 kg	
<b>Tower</b>	Height above ground	87.6 m	
	Overall (Integrated) Mass	347460 kg	
	1-st Side-to-Side Mode Natural Frequency	0.32 Hz	
	Structural-Damping Ratio	1%	
	TMD Mass Ratio	1%	
	TMD Damping Ratio	6.09%	

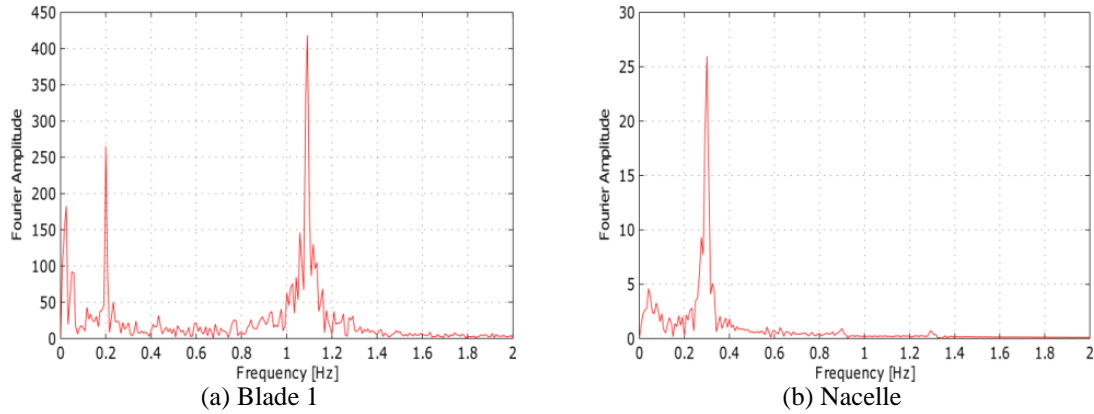


Fig. 4 Fourier amplitude of displacement response

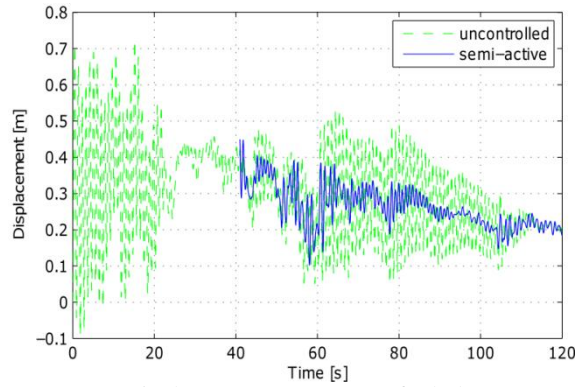
In order to assess the effectiveness of the semi-active algorithm, the main parameters of the system were varied over time to determine if the STMDs could adjust for these changes in system dynamics. The parameters considered were:

1. the rotational speed of the blades,  $\Omega$
2. the natural frequency of the blades,  $\omega_b$
3. the natural frequency of the nacelle,  $\omega_{nac}$

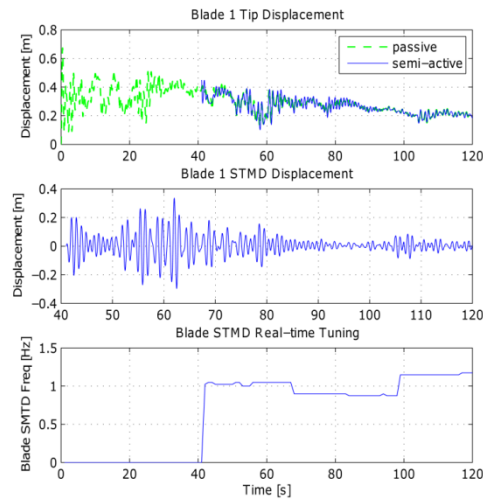
In each set of results, the undamped and semi-active responses are plotted to see the effect of the algorithm. The simulations run for an initial period of 41 seconds with just passive tuning and the STFT algorithm is then activated. This is to facilitate the collection of data for the first time of 40 seconds needed for the STFT computations. This results in a frequency step of 0.025 Hz ensuring accurate tuning of the STMDs. During the passive phase, the STMDs are kept inactive allowing the real-time tuning of the dampers to be seen when the semi-active algorithm is initiated. In the first set of numerical experiments the dynamics of the wind turbine without the contribution from the gravitational force are simulated, in order to separately study the response of the structure subjected to wind loadings. Subsequently, the effect of gravity is included, which is shown to have a substantial impact when large wind turbines and low rotational speed are considered. Finally, the performances of the proposed controller are tested on a parked wind turbine model subjected to extreme winds.

### 3.1 Varying $\Omega$ , the rotational speed of the blades

Variation in the rotational speed,  $\Omega$ , was first investigated slowing down from 0.202 Hz to 0.118 Hz over 120 seconds. Fig. 5(a) shows the undamped and damped blade response. Initially an increase is seen in the response of the blade when the TMD tunes at  $t = 41$ s. However a remarkable reduction in the edgewise displacement of the blade is achieved once the TMD settles down. The behaviour of the blade STMD is shown in Fig. 5(b). As can be observed the damper is initially detuned until the STFT algorithm initiates and then tunes in real-time to the dominant frequency in the response, hence achieving the reduction in Fig. 5(a).



(a) Displacement Response of Blade 1

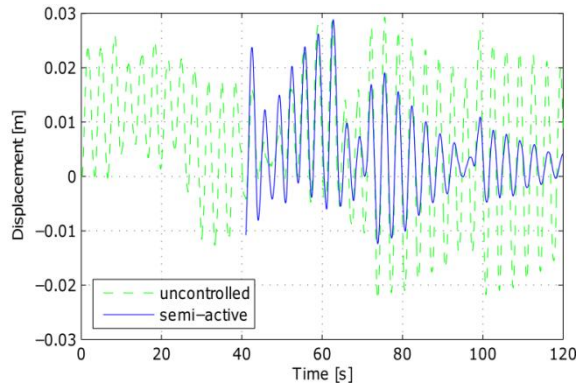


(b) Blade 1 STMD behaviour and tuning

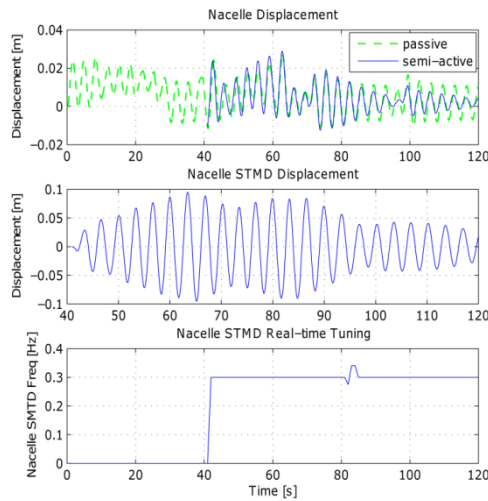
Fig. 5 Blade 1 semi-active control, varying  $\Omega$ Table 2 Performance of the edgewise response control for varying  $\Omega$ 

	Blade 1			Nacelle		
	Uncontrolled	Passive	Semi-active	Uncontrolled	Passive	Semi-active
Max Displacement [m]	0.5319	0.4187	0.4495	0.0293	0.0267	0.0288
RMS Displacement [m]	0.2818	0.2688	0.2689	0.0139	0.0091	0.0088
Max Velocity [ $\text{ms}^{-1}$ ]	1.5308	0.7416	0.8065	0.0530	0.0351	0.0375
RMS Velocity [ $\text{ms}^{-1}$ ]	0.6146	0.1526	0.1834	0.0242	0.0137	0.0134

The time history response for the nacelle is shown in Fig. 6(a) with the corresponding STMD behaviour shown in Fig. 6(b). A reduction of up to 50% is consistently achieved in the response when the control algorithm initiates. A numerical comparison of the performances achieved by the TMDs and STMDs for the case considered is provided in Table 2.



(a) Displacement Response Nacelle



(b) Nacelle STMD behaviour and tuning

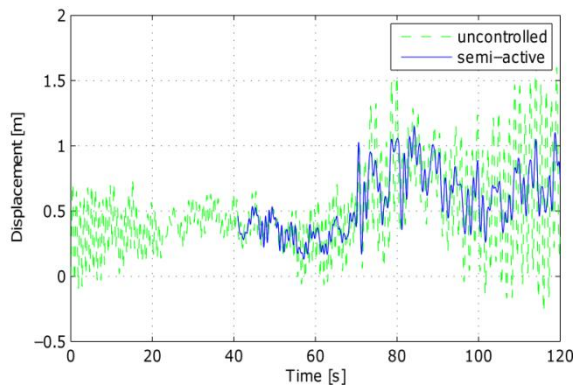
Fig. 6 Nacelle semi-active control, varying  $\Omega$

### 3.2 Varying blade natural frequency, $\omega_b$

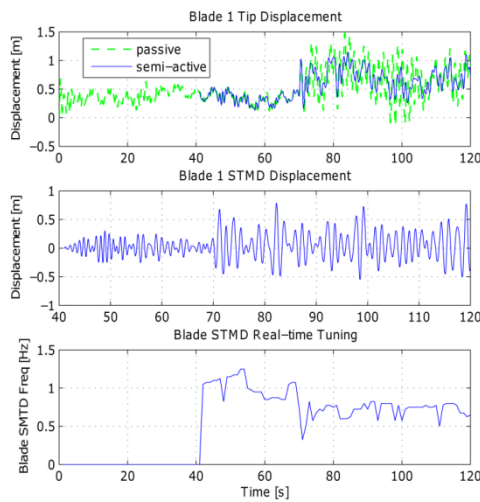
Variation in the natural frequency of blade 1,  $\omega_{b1}$ , from 1.09 Hz to 0.76 Hz was assumed at a time,  $t = 70$ s. The response of blade 1 is plotted in Fig. 7(a) with the corresponding STMD behaviour illustrated in Fig. 7(b). A reduction is seen both before and after the change in blade natural frequency due to the algorithm's ability to adjust the tuning of the STMD. As can be seen in Fig. 7(b), at  $t = 70$ s the STMD retunes to the new dominant frequency. The STMD performances

are also compared with a passive TMD tuned at the blade natural frequency. The adaptive capabilities of the semi-active algorithm allow track the new dominant frequency and hence to achieve a significant improvement in the vibration control when the parametric change occurs.

Fig. 8(a) shows the corresponding displacement response of the nacelle. Again a significant reduction in response is seen both before and after the loss in blade stiffness. Despite no change occurring in the nacelle properties the coupling present in the system from the blades results in a change in the nacelle STMD tuning when the loss in blade stiffness occurs. This can be observed in Fig. 8(b). A summary of the performances of blade 1 and nacelle responses is shown in Table 3. It can be observed that in this case the adaptive capabilities of the semi-active tuned mass damper provide better results for the blade response. This is due to the re-tuning of the STMDs after the variation in  $\omega_b$ .

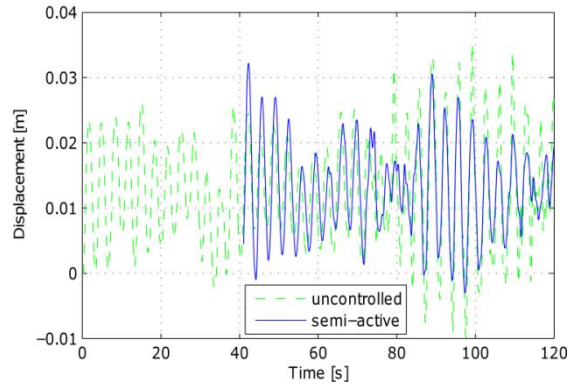


(a) Displacement Response of Blade 1

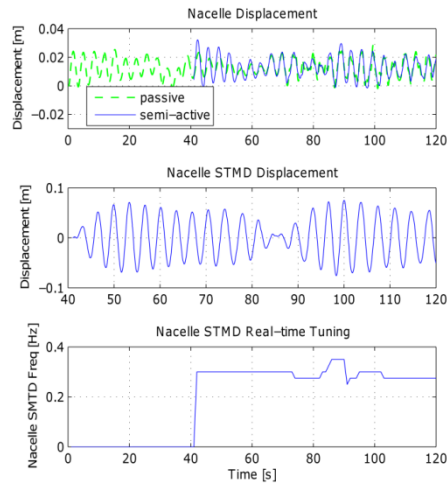


(b) Blade 1 STMD behaviour and tuning

Fig. 7 Blade 1 semi-active control, varying  $\omega_b$



(a) Displacement Response Nacelle



(b) Nacelle STMD behaviour and tuning

Fig. 8 Nacelle semi-active control, varying  $\omega_b$

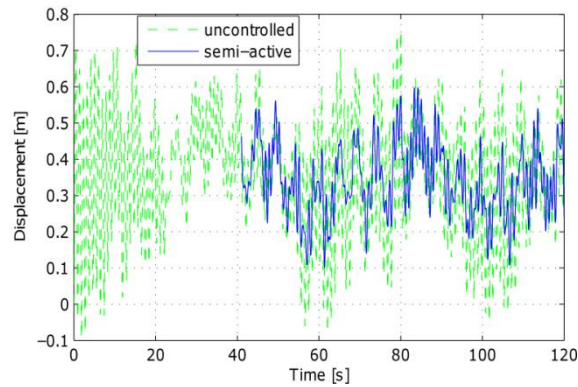
Table 3 Performance of the edgewise response control for varying  $\omega_b$

	Blade 1			Nacelle		
	Uncontrolled	Passive	Semi-active	Uncontrolled	Passive	Semi-active
Max Displacement [m]	1.6979	1.4898	1.1480	0.0352	0.0284	0.0322
RMS Displacement [m]	0.6783	0.6493	0.6160	0.0157	0.0142	0.0148
Max Velocity [ $\text{ms}^{-1}$ ]	4.1001	3.1301	1.7466	0.0602	0.0385	0.0354
RMS Velocity [ $\text{ms}^{-1}$ ]	1.5513	1.0220	0.4615	0.0197	0.0128	0.0134

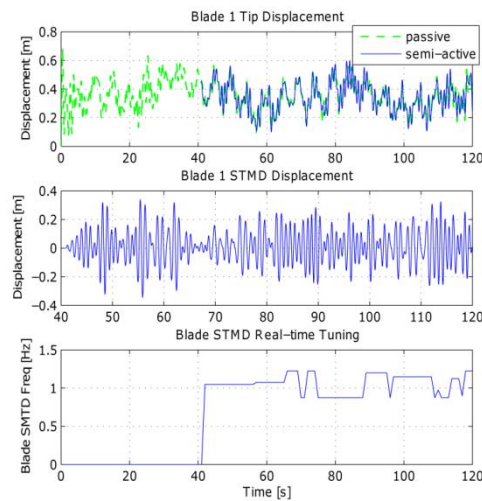
### 3.3 Varying nacelle natural frequency, $\omega_{nac}$

Finally, variation in nacelle natural frequency,  $\omega_{nac}$ , from 0.32 Hz to 0.24 Hz was assumed, again at  $t = 70$ s. Fig. 9(a) shows the blade response. As can be seen a reduction in peak to peak displacement is achieved both before and after the change in the nacelle natural frequency highlighting the tracking capability of the STMD. The blade STMD behaviour is plotted in Fig. 9(b).

The nacelle response is shown in Fig. 10(a) with the corresponding STMD behaviour plotted in Fig. 10(b). When the loss in nacelle stiffness occurs the STMD is seen to adjust its tuning to cater for the new system behaviour after  $t = 70$ s. As expected a good reduction in response is again achieved. Further, an improvement with respect to the passive TMD (first tuned at the nacelle natural frequency) is observed once the STMD settles down.

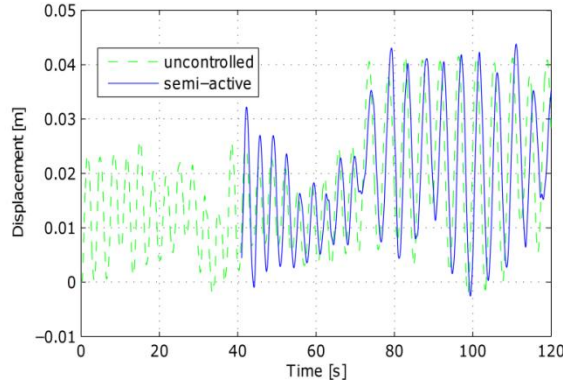


(a) Displacement Response of Blade 1

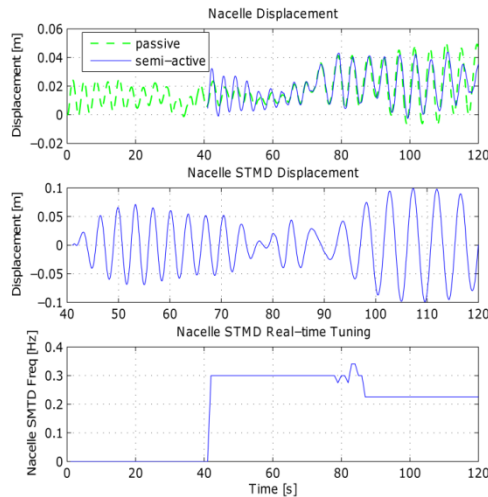


(b) Blade 1 STMD behaviour and tuning

Fig. 9 Blade 1 semi-active control, varying  $\omega_{nac}$



(a) Displacement Response Nacelle

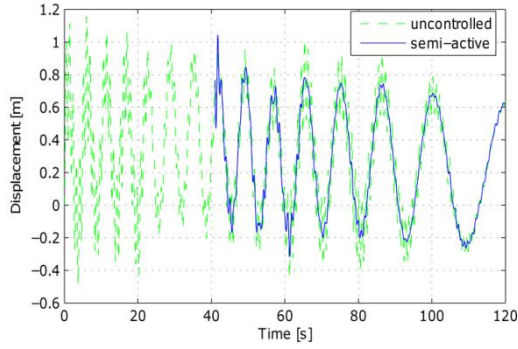


(b) Nacelle STMD behaviour and tuning

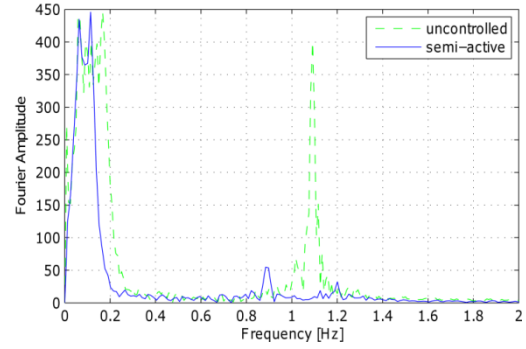
Fig. 10 Nacelle semi-active control, varying  $\omega_{nac}$

### 3.4 Edgewise model with gravity

The wind turbine model derived for this study was extended to include the effect of gravity on the dynamics of the edgewise vibration. The same simulation scenarios described previously have been considered, with changes in the rotational speed and the fundamental frequency of the blade and the nacelle, respectively. The time history of blade 1 tip displacement under variation of the rotor speed  $\Omega$  is shown in Fig. 11(a). A reduction in the high frequencies affecting the undamped response is observed. This is clearly seen in the corresponding Fourier spectrum (Fig. 11(b)), which shows a substantial suppression of the peak associated with the natural frequency of the blade. An improvement in the nacelle response is also achieved by the semi-active controller (Figs. 12(a) and 12(b)).

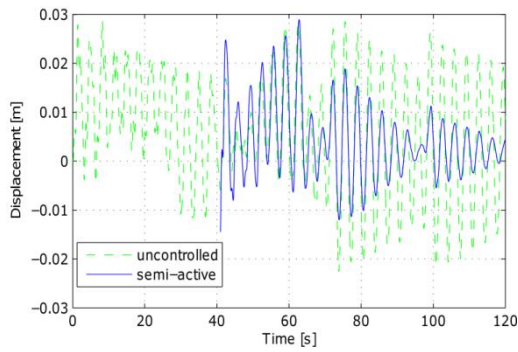


(a) Displacement Response of Blade 1

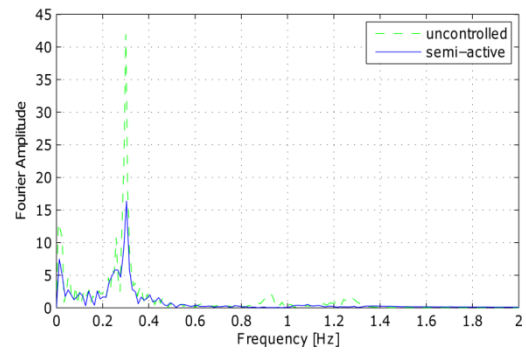


(b) Frequency content of Blade 1 Response

Fig. 11 Blade 1 semi-active control, varying  $\Omega$  (model with gravity)

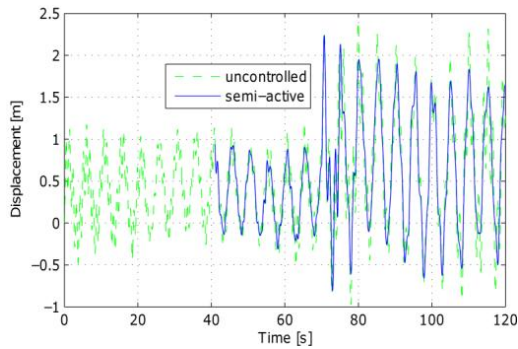


(a) Displacement Response of Nacelle

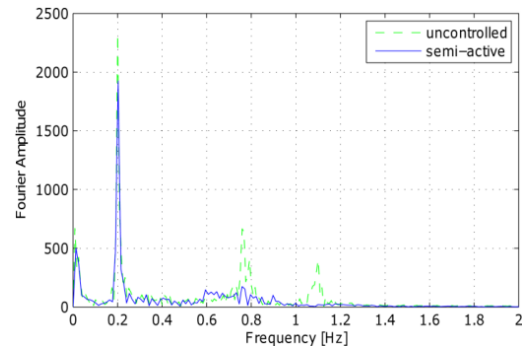


(b) Frequency Content of Nacelle Response

Fig. 12 Nacelle semi-active control, varying  $\Omega$  (model with gravity)



(a) Displacement Response of Blade 1



(b) Frequency content of Blade 1 Response

Fig. 13 Blade 1 semi-active control, varying  $\omega_b$  (model with gravity)

A step change in the fundamental frequency  $\omega_b$  of the blade was simulated at  $t=70$ s. Also in this case, the STMD is capable to adapt to the new conditions by tracking around the blade natural frequency, thus leading to a reduction in the vibrational response of the blade (Fig. 13(a)) and the nacelle (Figs. 14(a) and 14(b)). Although, due to the gravitational effect, most of the energy is concentrated in the band around the peak associated with the rotor speed (which is also the generalized load frequency), Fig. 13(b) shows the suppression of the peaks corresponding to the natural frequencies of the blade and also a mitigation of the peak around 0.2 Hz for the controlled response.

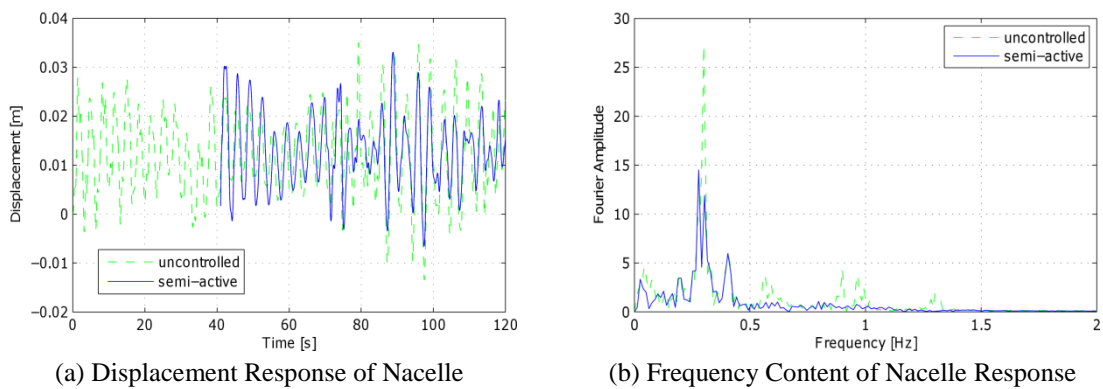


Fig. 14 Nacelle semi-active control, varying  $\omega_b$  (model with gravity)

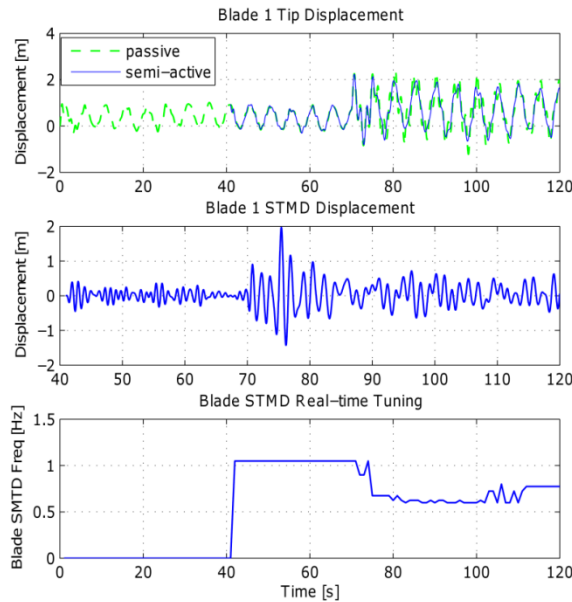


Fig. 15 Blade 1 STMD behaviour and tuning, varying  $\omega_b$  (model with gravity)

When the structural variation in the blade occurred at  $t=70$ s, the STFT algorithm allowed to detect the change in the dominant frequency (Fig. 15) and the stiffness of the damper was appropriately controlled to cater for the new conditions.

Finally, a loss in the stiffness of the nacelle was simulated. Once again at  $t=70$  s the parametric change occurred and the application of the semi-active controller resulted in an improvement of the responses, as shown in Figs. 16-18.

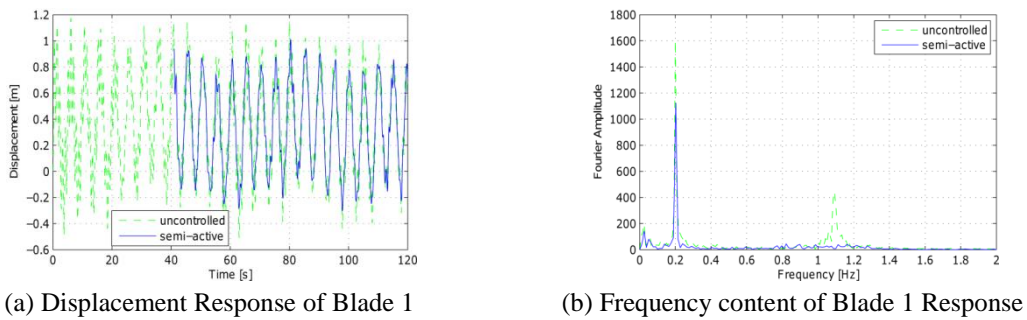


Fig. 16 Blade 1 semi-active control, varying  $\omega_{nac}$  (model with gravity)

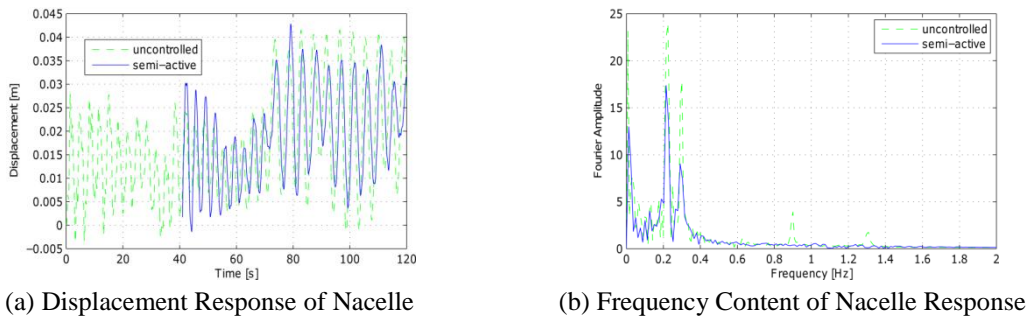


Fig. 17 Nacelle semi-active control, varying  $\omega_{nac}$  (model with gravity)

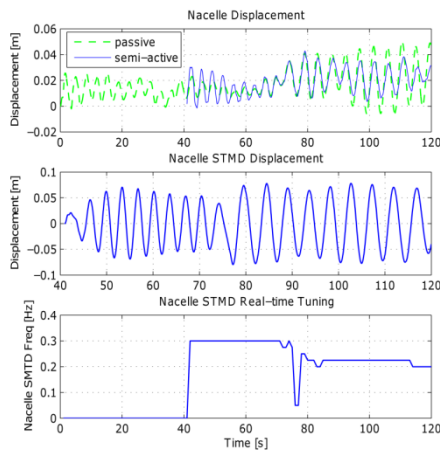


Fig. 18 Nacelle STMD behaviour and tuning, varying  $\omega_{nac}$  (model with gravity)

### 3.5 Parked wind turbine case

The performances of the semi-active controller have also been tested on a parked wind turbine model subjected to extreme winds. Under this condition, the rotor is in an idle state and no power is generated from the turbine. For instance, the blades are pitched to a parked position when the wind speed exceeds a certain value, namely the “cut-out” speed, in order to prevent damages to the generator and ensure the structural safety of the system. In this case, even though the power plant is not operating, the mechanical components have to cope with the loads resulting from high winds and the blades might experience very high loads and large amplitude edgewise vibrations. In a parked situation, instability issues due to stall-induced vibrations may also arise (Hansen 2007). In the numerical simulations carried out in this study, a mean wind speed of 45 m s<sup>-1</sup> with a strong (30% intensity) turbulent component was considered, in order to assess the effectiveness of the proposed control strategy in damping structural vibrations under extreme winds conditions.

The behaviour of the system in case of a loss in stiffness of the blade was analyzed first. A significant reduction of the edgewise vibration was achieved for the blade (Figs. 19(a) and 19(b)) and the nacelle (Figs. 20(a) and 20(b)) both before and after the variation of  $\omega_b$  at  $t=70$  s for the first blade. In particular, Fig. 19(b) shows that the two distinct peaks corresponding to the blade natural frequencies were successfully eliminated in the controlled response.

Since the STMD was adaptively tuned, it was again able to overcome the performances of the passive TMD once the latter became mistuned due to the variation in  $\omega_b$  (Fig. 21).

Finally, a variation  $\omega_{nac}$  was simulated. The results for this simulation are shown in (Figs. 22-24). Again, a significant improvement in the responses of the blade and the nacelle was achieved.

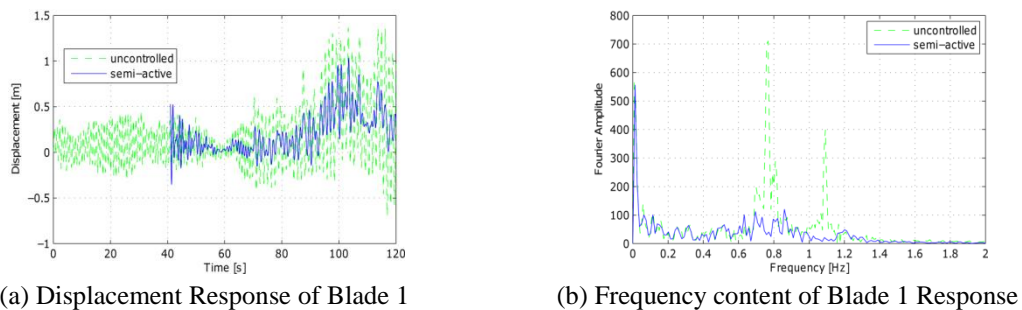


Fig. 19 Blade 1 semi-active control, varying  $\omega_b$  (parked wind turbine)

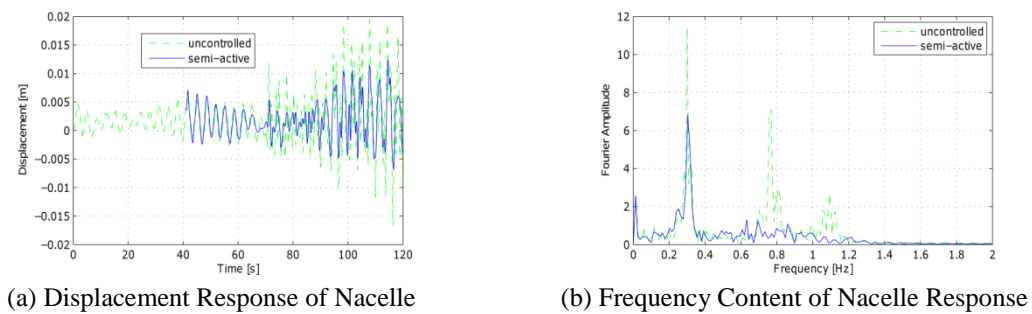


Fig. 20 Nacelle semi-active control, varying  $\omega_b$  (parked wind turbine)

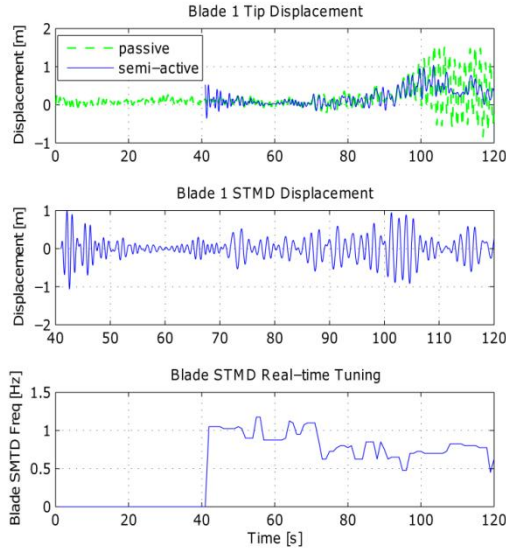
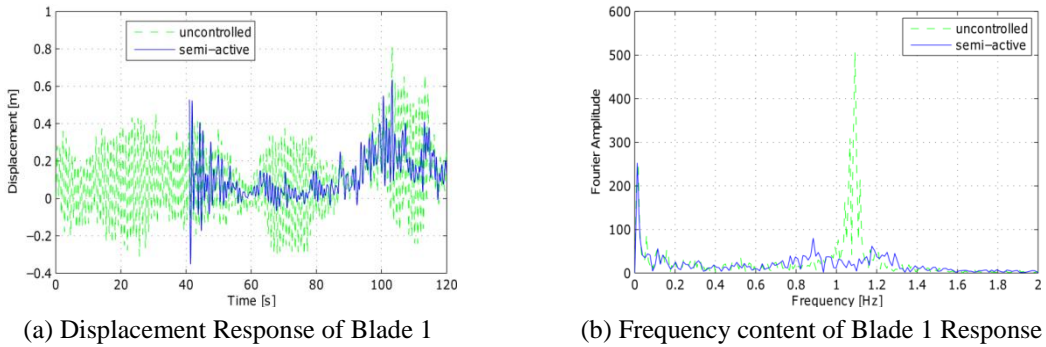


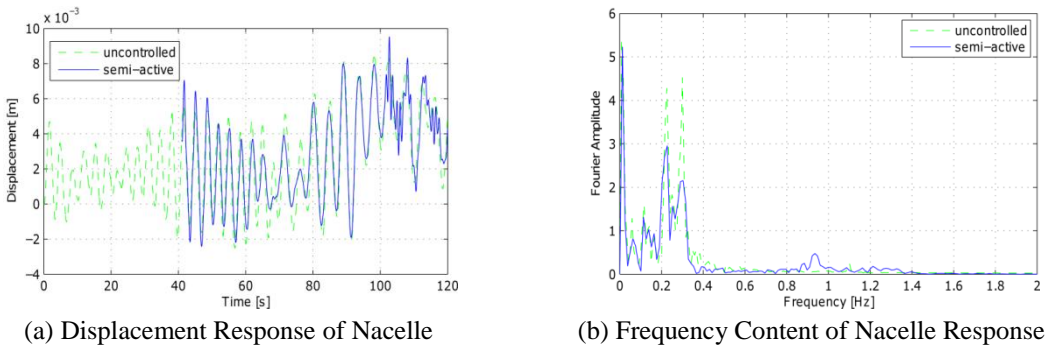
Fig. 21 Blade 1 STMD behaviour and tuning, varying  $\omega_b$  (parked wind turbine)



(a) Displacement Response of Blade 1

(b) Frequency content of Blade 1 Response

Fig. 22 Blade 1 semi-active control, varying  $\omega_{nac}$  (parked wind turbine)



(a) Displacement Response of Nacelle

(b) Frequency Content of Nacelle Response

Fig. 23 Nacelle semi-active control, varying  $\omega_{nac}$  (parked wind turbine)

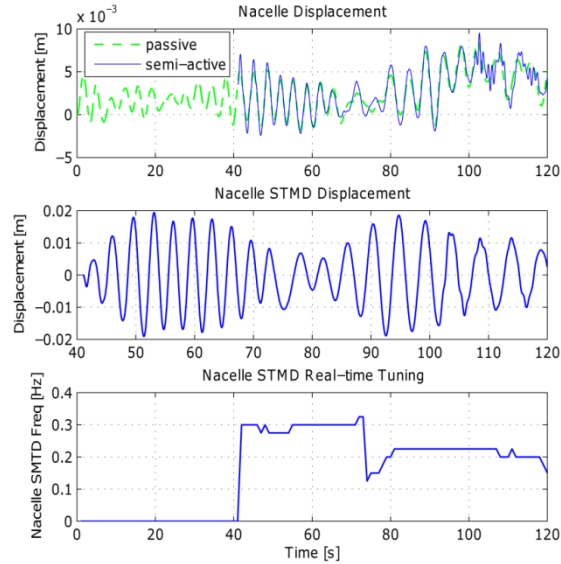


Fig. 24 Nacelle STMD behaviour and tuning, varying  $\omega_{nac}$  (parked wind turbine)

## 5. Conclusions

The use of an STFT algorithm for the semi-active control of edgewise vibrations in wind turbine blades has been investigated in this paper. The time history response of the model was split up into short segments, each of which were Fourier analysed, allowing the frequency content of the system to be determined with respect to time. The STMDs were then tuned in real-time to the current dominant frequency in the system. A Hanning window was employed highlighting the frequencies near the current time giving more emphasis to the ‘local’ frequency peaks. Variation in the dynamic behaviour of the system was studied. The parameters considered were the rotational speed,  $\Omega$ , the blade natural frequency,  $\omega_b$ , and the nacelle’s natural frequency,  $\omega_{nac}$ .

The behaviour of the system subjected to aerodynamic loads only and aerodynamic loads with gravity have been investigated. Further, the application of the semi-active control algorithm for a parked wind turbine model under extreme wind speeds has been examined.

A fine sampling frequency was used in the algorithm to achieve accurate tuning of the dampers. This was achieved by initially letting the system run for 41 seconds before activating the STFT control algorithm. This allowed a frequency step of 0.025 Hz resulting in accurate tuning to the frequency peaks.

In conclusion, the use of semi-active TMDs for edgewise vibration control of wind turbine blades has been shown to be feasible. The use of the STFT algorithm developed in this paper allows for real-time tuning of the STMDs to the dominant frequencies in the system. A remarkable reduction is achieved in both the nacelle and the blades by the inclusion of STMDs at the relevant degrees of freedom. The STFT algorithm developed has been shown to be effective for a 5-MW turbine with realistic structural and aerodynamic properties subjected to a turbulent wind load (both under operating and parked conditions). Promising results for parked conditions are worth a special mention as edgewise vibration can be a major concern in this case.

## Acknowledgments

The authors would like to thank Professor Søren R. K. Nielsen for his advice regarding the model formulation. Funding for this work was provided by the Irish Research Council for Science, Engineering and Technology (IRCSET), the Marine Institute under the Networking and Technology Transfer Initiative and the EU FP7 funding for the Marie Curie ITN project SYSWIND (Grant No. PITN-GA-2009-238325).

## References

- Ahlström, A. (2006), "Influence of wind turbine flexibility on loads and power production", *Wind Energy*, **9**(3), 237-249.
- Arrigan, J., Pakrashi, V., Basu, B. and Nagarajaiah, S. (2011), "Control of flapwise vibrations in wind turbine blades using semi-active tuned mass dampers", *Struct. Control Health Monit.*, **18**(8), 840-851.
- Bechly, M.E. and Clausen, P.D. (1997), "Structural design of a composite wind turbine blade using finite element analysis", *Comput. Struct.*, **63**(3), 639-646.
- Chang, C.C. (1999), "Mass dampers and their optimal designs for building vibration control", *Eng. Struct.*, **21**(5), 454 - 463.
- Chaviaropoulos, P.K. (2001), "Flap/lead-lag aeroelastic stability of wind turbine blades", *Wind Energy*, **4**(4), 183-200.
- Chaviaropoulos, P.K., Nikolaou, I.G., Aggelis, K.A., Sørensen, N.N., Johansen, J., Hansen, M.O.L., Gaunaa, M., Hambræus, T., von Geyr, H.F., Hirsch, C., Shun, K., Voutsinas, S.G., Tzabiras, G., Perivolaris, Y. and Dyrmoose, S.Z. (2003), "Viscous and aeroelastic effects on wind turbine blades. The VISCEL project. Part I: 3D Navier-Stokes rotor simulations", *Wind Energy*, **6**(4), 365-385.
- Chaviaropoulos, P.K., Politis, E.S., Lekou, D.J., Sørensen, N.N., Hansen, M.H., Bulder, B.H., Winkelaar, D., Lindenburg, C., Saravanos, D.A., Philippidis, T.P., Galiotis, C., Hansen, M.O.L. and Kossivas, T. (2006), "Enhancing the damping of wind turbine rotor blades, the DAMPBLADE project", *Wind Energy*, **9**(1-2), 163-177.
- Cohen, L. (1995), *Time-frequency analysis*, Prentice-Hall, Inc., Upper Saddle River, NJ, USA.
- Hansen, M.H. (2003), "Improved modal dynamics of wind turbines to avoid stall-induced vibrations", *Wind Energy*, **6**(2), 179-195.
- Hansen, M.H. (2007), "Aeroelastic instability problems for wind turbines", *Wind Energy*, **10**(6), 551-577.
- Hansen, M.O.L. (2008), *Aerodynamics of wind turbines*, Earthscan.
- Hijmissen, J. and van Horssen, W. (2007), "On aspects of damping for a vertical beam with a tuned mass damper at the top", *Nonlinear Dynam.*, **50**, 169-190.
- Jensen, F.M., Falzon, B.G., Ankersen, J. and Stang, H. (2006), "Structural testing and numerical simulation of a 34 m composite wind turbine blade", *Compos. Struct.*, **76**(1-2), 52 - 61.
- Jonkman, J.M., Butterfield, S., Musial, W. and Scott, G. (2009), *Definition of a 5-MW reference wind turbine for offshore system development*, National Renewable Energy Laboratory, Technical report NREL/TP-500-38060, Golden, Colorado.
- Kaimal, J.C., Wyngaard, J.C., Izumi, Y. and Coté, O.R. (1972), "Spectral characteristics of surface-layer turbulence", *Q. J. Roy. Meteor. Soc.*, **98**(417), 563-589.
- Kareem, A. and Kline, S. (1995), "Performance of multiple mass dampers under random loading", *J. Struct. Eng. - ASCE*, **121**(2), 348-361.
- Lackner, M.A. and Rotea, M.A. (2011), "Passive structural control of offshore wind turbines", *Wind Energy*, **14**(3), 373-388.
- Li, H.N. and Ni, X.L. (2007), "Optimization of non-uniformly distributed multiple tuned mass damper", *J. Sound Vib.*, **308**(1-2), 80 - 97.

- Murtagh, P.J., Basu, B. and Broderick, B.M. (2005), "Along-wind response of a wind turbine tower with blade coupling subjected to rotationally sampled wind loading", *Eng. Struct.*, **27**(8), 1209 - 1219.
- Murtagh, P.J., Ghosh, A., Basu, B. and Broderick, B.M. (2008), "Passive control of wind turbine vibrations including blade/tower interaction and rotationally sampled turbulence", *Wind Energy*, **11**(4), 305-317.
- Nagarajaiah, S. (2009), "Adaptive passive, semiactive, smart tuned mass dampers: identification and control using empirical mode decomposition, Hilbert transform, and short-term Fourier transform", *Struct. Control Health Monit.*, **16**(7-8), 800-841.
- Nagarajaiah, S. and Basu, B. (2009), "Output only modal identification and structural damage detection using time frequency & wavelet techniques", *Earthq. Eng. Eng. Vib.*, **8**, 583-605.
- Nagarajaiah, S. and Sonmez, E. (2007), "Structures with semiactive variable stiffness single/multiple tuned mass dampers", *J. Struct. Eng. - ASCE*, **133**(1), 67-77.
- Nagarajaiah, S. and Varadarajan, N. (2005), "Short time Fourier transform algorithm for wind response control of buildings with variable stiffness TMD", *Eng. Struct.*, **27**(3), 431-441.
- Pinkaew, T. and Fujino, Y. (2001), "Effectiveness of semi-active tuned mass dampers under harmonic excitation", *Eng. Struct.*, **23**(7), 850 -856.
- Ronold, K.O. and Larsen, G.C. (2000), "Reliability-based design of wind-turbine rotor blades against failure in ultimate loading", *Eng. Struct.*, **22**(6), 565 -574.
- Ronold, K.O., Wedel-Heinen, J. and Christensen, C.J. (1999), "Reliability-based fatigue design of wind-turbine rotor blades", *Eng. Struct.*, **21**(12), 1101- 1114.
- Shokrieh, M.M. and Rafiee, R. (2006), "Simulation of fatigue failure in a full composite wind turbine blade", *Compos. Struct.*, **74**(3), 332 - 342.
- Simiu, E. and Scanlan, R.H. (1996), *Wind effects on structures: fundamentals and applications to design*. Wiley-Interscience publication. John Wiley.
- Staino, A. and Basu, B. (2011), "Robust constrained model predictive control for flapwise vibrations mitigation in wind turbines", (Eds. Roeck, G. D., Degrande, G., Lombaert, G. and Müller, G.), *Proceedings of the 8th International Conference on Structural Dynamics, EURO-DYN 2011*.
- Staino, A., Basu, B. and Nielsen, S.R.K. (2012), "Actuator control of edgewise vibrations in wind turbine blades", *J. Sound Vib.*, **331**(6), 1233- 1256.
- Thomsen, K., Petersen, J.T., Nim, E., Øye, S. and Petersen, B. (2000), "A method for determination of damping for edgewise blade vibrations", *Wind Energy*, **3**(4), 233-246.